Geophys. J. Int. (2004) **157,** 305–314 doi: 10.1111/j.1365-246X.2004.02202.x

Surface wave waveform inversion for variation in upper mantle structure beneath Iceland

Zhijun Du[1] and G. R. Foulger[2]

[1] *Institute of Theoretical Geophysics, University of Cambridge, Cambridge* CB2 3EQ, *UK. E-mail: Zhijun.Du@itg.cam.ac.uk*
[2] *Department of Geological Sciences, University of Durham, South Road, Durham* DH1 3LE, *UK. E-mail: G.R.Foulger@durham.ac.uk*

Accepted 2003 November 21. Received 2003 November 17; in original form 2002 June 13

SUMMARY

We study the structure of the upper mantle beneath Iceland using surface wave waveforms recorded at pairs of stations lying approximately on the same great circles as the sources used. We invert for local, path-average V_s variations between the station pairs. The method used in this study is an extension of an algorithm proposed by Kushnir *et al.* (1989), which uses only the phase of the seismograms. In our waveform inversion not only the phases but also the amplitudes of the surface waves are used as structural constraints. We illustrate the resolution power of the new algorithm with synthetic examples. We apply the method to study upper mantle structure beneath Iceland using recordings of three events with northerly, south-southwesterly and easterly orientated paths and 19 station pairs. Depending on the separation distance of the stations, we invert waveforms in the frequency range 0.0166–0.08 Hz and 0.01–0.08 Hz. Resolution is limited by the penetration depth of the surface wave fundamental mode, and is good down to ∼150 km for the narrower frequency band and ∼200 km for the wider band. Although the inversions of the differential waveforms only provide information on lateral V_s variations between station pairs, the main structural features of the upper mantle beneath Iceland are retrieved. We confirm that the strongest negative V_s anomalies of up to ∼ −5 per cent underlie central Iceland, and extend down to the limit of our resolution at ∼200 km. The rift zones away from central Iceland are underlain by low velocities in the depth range ∼50–100 km and high velocities below this, indicating that they are shallowly sourced. Such a structure also underlies northwest Vatnajokull, where a mantle plume is traditionally assumed to lie. Beneath intraplate areas, mantle structural variations are small. Using our method, smaller-scale mantle structures are detectable than is possible with teleseismic tomography, which tends to smear anomalies throughout larger volumes.

Key words: hotspot, Iceland, seismic structure, surface waves, upper mantle, waveform inversion.

1 INTRODUCTION

Whole-mantle seismic tomography images of the north Atlantic reveal a broad, low-wave-speed anomaly which occupies most of the region (e.g. Ritsema *et al.* 1999). Detailed study of the Iceland area itself has mainly been done so far using teleseismic tomography. For example, inversion of the arrival times of 3159 *P* waves and 1338 *S* waves recorded on a network of 35 digital, broad-band stations covering the whole of Iceland, including diffracted and core–mantle boundary phases, yielded mantle structure to a depth of ∼450 km (Foulger *et al.* 2000, 2001). Other teleseismic tomography studies of the Iceland region include those of Tryggvason *et al.* (1983), Wolfe *et al.* (1997) and Allen *et al.* (2002). All show low velocities underlying central Iceland and extending down to depths of 300–400 km. A comprehensive comparison of most of these, along with whole-mantle tomography images of the region, has been presented by Foulger *et al.* (2001). Such studies use relative seismic wave traveltimes, an approach that assumes that arrival time delays caused by structure outside the study region depend only on epicentral distance, and can be corrected using a 1-D standard Earth reference model such as PREM or IASP91. This approach yields estimates of regional Earth structure using a large set of long propagation paths. However, it suffers from the problems of large-volume averaging and underestimation of local velocity perturbations.

In this paper we extend a waveform inversion method first used by Kushnir *et al.* (1989) and apply it to study the structure of the upper mantle beneath Iceland. We rigorously subtract the effects of crustal structure using a whole-Iceland V_s structure derived using receiver functions (Du & Foulger 1999, 2001; Du *et al.* 2002; Foulger *et al.* 2003). We then invert for local mantle structure and average velocity gradients along interstation ray paths. By using short ray paths and full waveforms we achieve higher structural resolution

than is possible with teleseismic traveltime tomography, and detect regional structural details which are blurred by averaging in teleseismic tomography inversions. We find that intraplate parts of Iceland are underlain by mantle with little lateral variation, up to ∼2.5 per cent. Beneath the rift zones away from central Iceland, low-velocity anomalies of up to ∼3 per cent occur in the depth range ∼50–100 km. Beneath central Iceland low-velocity anomalies of up to ∼5 per cent extend down to ∼200 km, the approximate depth limit of our resolution.

2 METHOD

Kushnir *et al.* (1989) expressed surface wave propagation between two stations A and B, located on the same great circle as the source, as

$$U_{\mathrm{B}}(\omega) = \mathbf{H}(\omega, \mathbf{m})U_{\mathrm{A}}(\omega) \tag{1}$$

where $\mathbf{H}(\omega, \mathbf{m})$ represents the equivalent matrix frequency response of the medium relating the spectra of surface wave waveforms at the first (A) and second (B) station. For a horizontally homogeneous medium, $\mathbf{H}(\omega, \mathbf{m})$ is a function of the geometric divergence and anelastic damping of the waves between the two stations. Waveform inversion for such a simple case was first performed by Kushnir *et al.* (1989) and later by Passier *et al.* (1997), who applied the method to map V_{s} perturbations in the mantle beneath Australia.

For a smooth, laterally varying medium where the seismic parameters depend on the horizontal coordinates, $\mathbf{H}(\omega, \mathbf{m})$ can be described by its asymptotic 'local mode' approximation (Woodhouse 1974; Levshin 1985; Kennett 1995). This means that, in such a medium, surface wave propagation can be represented in terms of the contributions of the source and the path and receiver structures. In practice, vector harmonics can be used to expand a single modal eigenfunction for a single structure (e.g. the structure at the source) in terms of the orthogonal set of eigenfunctions for another structure (e.g. the structure at the receiver) (Maupin & Kennett 1987). However, the use of this approach to estimate changes in surface wave modal eigenfunctions is computationally expensive. Instead of using numerical harmonics, Du & Panza (1999) tackled the problem with an analytical formulism using differential seismograms, where the changes in modal eigenfunctions caused by structural model perturbations are calculated efficiently and accurately. Their method can be implemented directly in waveform inversions.

Here we consider the case where surface wave modes depend on the properties of the local medium beneath a pair of stations. For such a case, ray theory for surface waves is applicable. The properties of the medium beneath the pair of stations A and B can be expressed as

$$[U\sqrt{uIJ}/\varepsilon]_{\mathrm{B}} = [U\sqrt{uIJ}/\varepsilon]_{\mathrm{A}} \exp(-ik\Delta x) \tag{2}$$

where u, I and ε are local Rayleigh wave group velocity, energy integral and ellipticity respectively. J describes geometric spreading and Δx is the distance between the stations A and B. Eq. (2) was used by Levshin (1985) to estimate the effect of change in the amplitude of a surface wave in a weakly laterally inhomogeneous medium.

Given data U_{A} and U_{B}, eq. (1) constitutes a set of linear equations via $\mathbf{H}(\omega,\mathbf{m})$. We determine $\mathbf{H}(\omega, \mathbf{m})$ using (2). If we express the seismogram in the simple form $U(\omega) = t(\omega, \mathbf{m})c(\omega)$, we obtain

$$\begin{pmatrix} U_{\mathrm{A}}(\omega) \\ U_{\mathrm{B}}(\omega) \end{pmatrix} = U(\omega) = \begin{pmatrix} t(\omega, \mathbf{m}_{\mathrm{A}})c(\omega) \\ t(\omega, \mathbf{m})c(\omega) \end{pmatrix} \tag{3a}$$

where $c(\omega)$ is the source spectrum and $t(\omega, \mathbf{m})$ is the response of the medium. It is reasonable to assume that the source term, $c(\omega)$, is identical for both stations. At station A, the best estimate of $c(\omega)$ can be obtained by minimizing the function

$$\Gamma = \sum_{\omega_k} \| \mathbf{U}(\omega_k) - \mathbf{t}(\omega_k, \mathbf{m}_{\mathrm{A}})c(\omega_k) \|^2 . \tag{4}$$

When $\mathbf{m}_{\mathrm{A}}$ is given, Γ is a minimum if

$$\overline{c}(\omega_k) = \frac{\mathbf{t}^*(\omega_k)U(\omega_k)}{\mathbf{t}^*(\omega_k)t(\omega_k)} \tag{5}$$

where the asterisk denotes the complex conjugate. Here, $\overline{c}(\omega)$ designates the optimum estimate of the source excitation parameters. It is important to note here that $\overline{c}(\omega)$ also includes the effects of wave propagation through the medium between the source and the near station (A).

By substituting eq. (5) back into (4), replacing $\mathbf{t}(\omega_{\mathrm{k}}, \mathbf{m}_{\mathrm{A}})$ with $\mathbf{t}(\omega_k, \mathbf{m})$, and minimizing Γ again, the model (or model vector $\mathbf{m}$) that best fits the waveform at the far station (B), within a pre-assigned frequency band, can be found.

3 SYNTHETIC TEST

The waveform inversion method of Kushnir *et al.* (1989) is adequate only where the differences in structure beneath the two stations result in a simple phase shift in the recorded surface waves, i.e. where the two structures are almost identical. The most important aspects and limits of such inversions have been discussed elsewhere (e.g. Kennett 1995; Du & Panza 1999). For laterally varying media, it is necessary to take into account the change in horizontal structure along the propagation path.

We compute seismograms using the structural models shown in Fig. 1(a). Model B has a ∼3–6 per cent higher velocity than Model A, which has relatively steep velocity gradients in the depth range 105–140 km. Although the overall velocity differences between the two models are small, the resulting synthetic seismograms are quite different. The two synthetic seismograms shown in Fig. 1(b) were computed at station A respectively using Models A and B, whereas Fig. 1(c) shows a synthetic seismogram for Model B computed at station B, which is 150 km distant from station A. Compared with the effects on the seismograms of the changes in the modal eigenfunctions resulting from the different structures (compare the two traces of Fig. 1b), the effect of wave dispersion (compare Fig. 1c with the lower trace of Fig. 1b) is small. We invert the synthetic seismograms shown in Fig. 1(b) (upper trace) and Fig. 1(c), assuming that the source parameters and receiver structures are unknown. We use both our method and that of Kushnir *et al.* (1989).

We start the inversions using the IASP91 standard Earth model as our initial model. Using eq. (5), we first fit the near station waveform (top trace, Fig. 1b) to obtain $\overline{c}(\omega)$. The fits to the near station A are good (Fig. 2), indicating good retrieval of the source term by both methods. We adopt $\overline{c}(\omega)$ at the far station and then invert the waveform at station B (Fig. 1c) to retrieve the structural variations between stations A and B. The inversion results are shown in Fig. 3. The method of Kushnir *et al.* (1989) computes the wavefield at station B, retaining the identity of the individual mode observed at station A, whereas we obtain the wavefield at station B from the surface wave 'local mode' approximation using (2). This takes into account the modal eigenfunction change of the structure between stations A and B.

The inversion method of Kushnir *et al.* (1989) considered $t(\omega, \mathbf{m})$ as a function of surface wave phase delay only, whereas we consider it to be a function of surface wave local modes, i.e. we also include the change of the seismogram amplitude (the change in

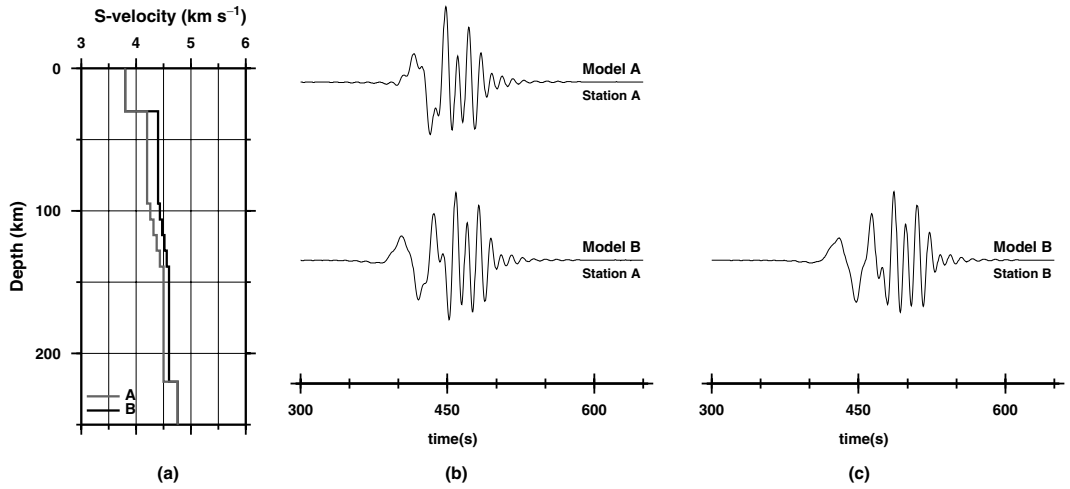

Figure 1. (a) *S*-wave velocity models A and B used to represent structures beneath stations A (near station) and B (far station). Stations A and B are assumed to lie on the same great circle as a source with epicentral distances of 1570 and 1720 km respectively. (b) Synthetic Rayleigh fundamental modes computed at station A using Model A (top) and B (bottom), and (c) same as bottom panel of (b) but computed for station B.

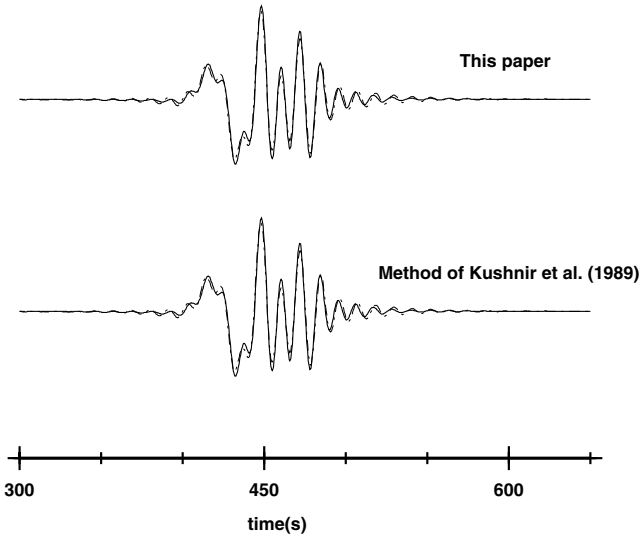

Figure 2. Fits to the 'observed' Rayleigh fundamental modes at near station A (top trace of Fig. 1b). The inversion was done using IASP91 as a starting model to retrieve the source term, $c(\omega)$, as described in the text. The solid lines are the 'observations', and the broken lines the synthetics. Top panel shows the result obtained using $c(\omega)$ derived using the method described in this paper, whereas the lower panel shows the result obtained using $c(\omega)$ derived by the method of Kushnir *et al.* (1989). The good fits show that both methods retrieve $c(\omega)$ well.

the modal eigenfunctions caused by structural differences between stations A and B). In Figs 4(a) and (b), we show the fits to the 'real' model by the two inversions, whereas in Fig. 4(c) we quantify the differences between the two inversions in terms of percentage difference [(i.e. 100× (inverted—'real')/'real']. Here the inverted model is the sum of Model A and the retrieved velocity variations (the bottom panels of Fig. 3) between stations A and B. Our inversion gives a difference of $\sim \pm 1$ per cent to a depth of ∼150 km, compared with a difference of up to $\sim \pm 3$ per cent yielded by the method of Kushnir *et al.* (1989). This means that ∼50 per cent of the pre-designated model differences were not retrieved using the method of Kushnir *et al.* (1989). It is clear that our new method not only fits the waveforms better (Fig. 3, upper panels) but it also retrieves structure significantly better. The use of the seismogram amplitude in waveform inversion in addition to the phase improves the quality of the structural result obtained.

At depths greater than 150 km, both methods retrieved the 'real' structure poorly (Fig. 4). This is a result of the limited penetration of the surface wave fundamental mode.

4 WAVEFORM INVERSION

In this section, we describe the results of waveform inversion of real data recorded in Iceland. We use three events with ray paths orientated northerly, easterly and south-southwesterly that sample most of the tectonic areas of Iceland (Fig. 5). The events and station pairs used lie on the same great circles. We inverted only the vertical component seismograms of the Rayleigh fundamental waves in the period ranges 12–60 and 12–100 s. These waves are sensitive to structure down to depths of ∼150 km and ∼200 km respectively. We chose the frequency band on the basis of station pair separations, with the wider frequency band being usable for the larger station separations (Table 1).

We invert the waveform difference between the two fundamental-mode Rayleigh wave waveforms to obtain relative V_s perturbations as a function of depth between the pairs of stations. We seek to derive mantle structure, and thus we correct for the crust using models from receiver functions and surface waves (Du & Foulger 1999, 2001; Du *et al.* 2002; Foulger *et al.* 2003). We then allow the excitation term, $c(\omega)$, to absorb the remaining differences in the crustal structure between the near and the far stations. We consequently achieved fits to the observations at or better than the ∼95 per cent level for our data for the near stations, down to periods as short as ∼12 s (Table 1). The few paths that were not fitted at the 95 percentile level after applying the corrections were excluded from the inversions.

Fig. 6 shows examples of waveform inversions for the station pairs HOT13–HOT22 (aligned northerly) and HOT14–HOT27 (aligned easterly). The period bands 12–100 s and 12–60 s respectively were used. The upper traces show the fit to the stations nearest the sources (HOT13 and HOT14) after retrieval of the source terms. The IASP91 model was used for the structure between the source and near stations. We correct IASP91 with the crustal models of stations HOT22

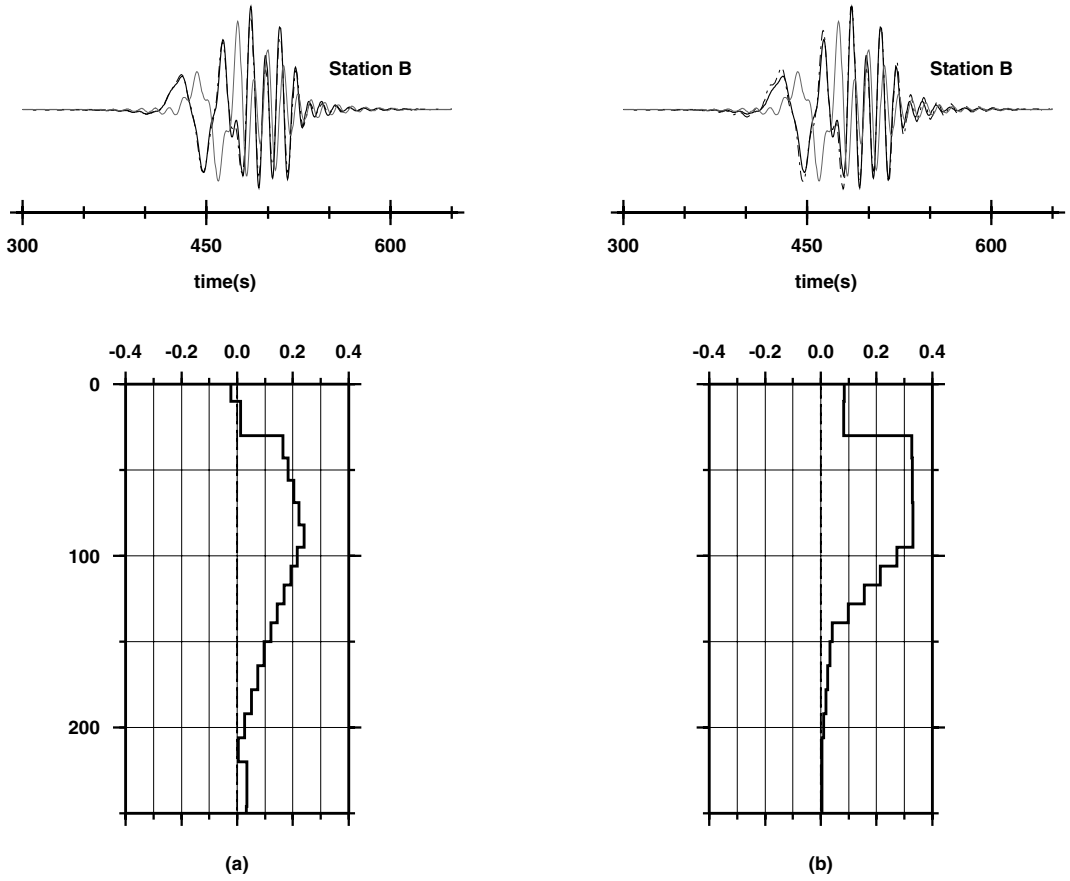

Figure 3. Results of waveform inversions conducted at far station B (Fig. 1c), using $c(\omega)$ obtained from inversion of the waveform of near station A. Upper panels: comparison of fits between waveforms obtained from the initial models (grey lines), the inversion results (broken lines), and the 'observed' seismograms (solid lines): (a) the fit obtained using the method described in this paper; (b) the result obtained using the method of Kushnir *et al.* (1989). Lower panels: retrieved V_S perturbations: (a) using the method described in this paper; (b) using the method of Kushnir *et al.* (1989).

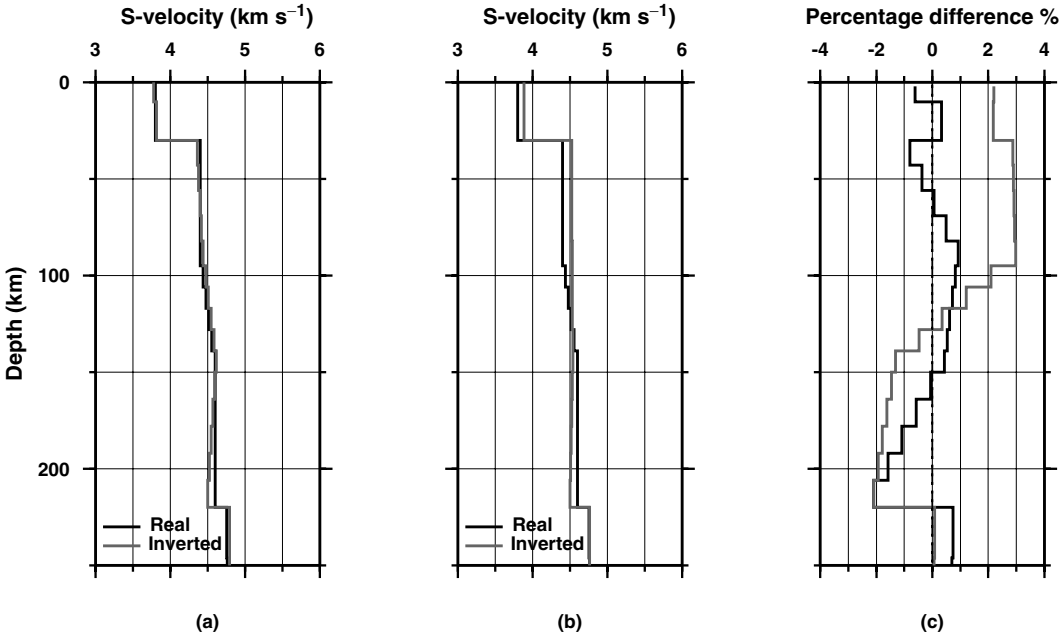

Figure 4. Comparison of the inversion results. The 'real' model is plotted as black lines both in (a) and (b), whereas the inverted models are shown as grey lines in (a) obtained by using the method described in this paper, and (b) obtained by using the method of Kushnir *et al.* (1989). (c) Percentage differences between the 'real' and inverted models. Solid line shows the result using the method described in this paper, grey line shows the result using the method of Kushnir *et al.* (1989).

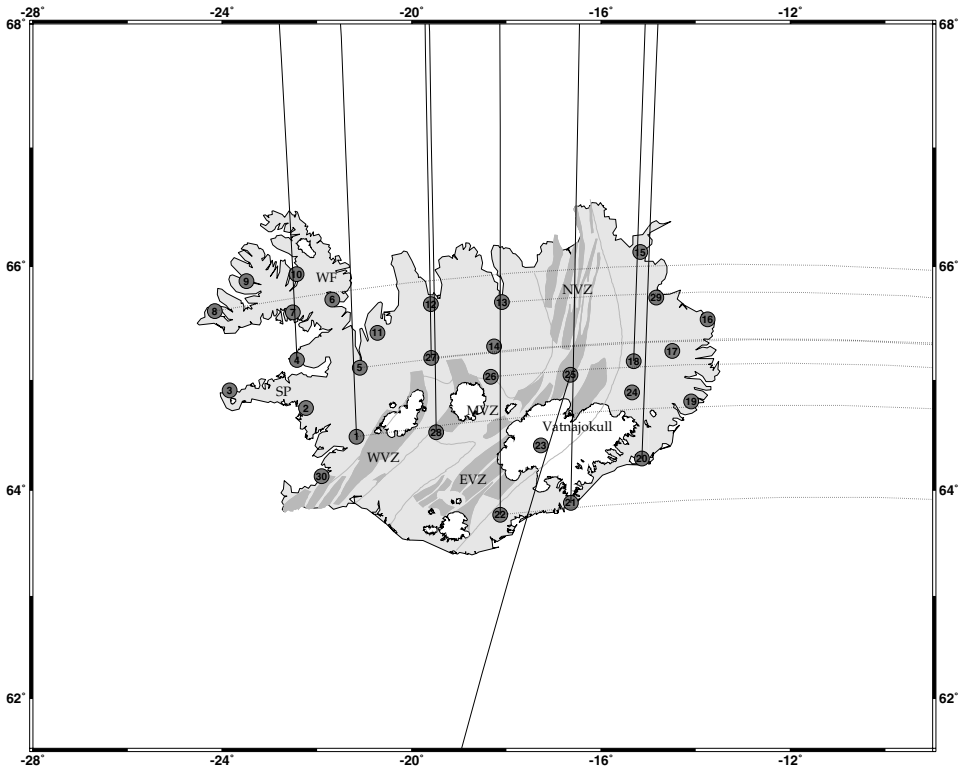

Figure 5. Great circle paths of earthquake waves used for waveform inversion to obtain upper mantle structure beneath Iceland. Circles show stations of the Iceland Hotspot Project, along with their station numbers. WF, Northwest Fjords; WVZ, EVZ, MVZ, NVZ, Western, Eastern, Middle and Northern Volcanic Zones; SP, Snaefellsnes peninsula. Grey zones are spreading centres that comprise the spreading plate boundary in Iceland and white are icecaps.

Table 1. Statistical fits to the data and period bands of data used in the inversions for different paths.

Path	Near station	Crustal model fit percentile	Period band used in inversion (s)
North–South			
HOT10–04	HOT10	98	12–60
HOT05–01	HOT05	96	12–60
HOT15–20	HOT15	96	12–100
HOT15–18	HOT15	97	12–60
HOT24–20	HOT24	98	12–60
HOT12–28	HOT12	96	12–100
HOT13–22	HOT13	98	12–100
HOT12–27	HOT12	99	12–60
HOT25–21	HOT25	96	12–100
HOT23–25	HOT23	97	12–60
East–West			
HOT06–08	HOT06	99	12–60
HOT27–05	HOT27	97	12–60
HOT14–27	HOT14	96	12–60
HOT14–05	HOT14	96	12–100
HOT21–22	HOT21	98	12–60
HOT18–26	HOT18	96	12–100
HOT29–13	HOT29	96	12–60
HOT28–01	HOT28	96	12–60
HOT19–28	HOT19	96	12–100

and HOT27 (Du & Foulger 2001; Du *et al.* 2002) for the paths HOT13–HOT22 and HOT14–HOT27 respectively. We inverted for the V_s differences from the reference models at the far stations to obtain the lateral variations between the station pairs. Because the inversions were conducted using the waveforms recorded at the near stations as input, the inversion results contain the V_s mantle structural differences between the near and far stations, i.e. path average V_s differences between the station pairs. The lower traces of Fig. 6 show the final fits for the far stations (HOT22 and HOT27) after the waveform inversions.

Although we have illustrated the structural resolution power of our inversion in Section 3 through synthetic examples, several aspects of the inversion of real data may also affect the resolution of the inversion. The diameter of the resolution kernel of the inversion using the wider frequency band is larger than that of using the narrower frequency band. The resulting error may be assessed by the statistical fit to the data, and the repeatability between comparable results. Path HOT14–HOT05 (eastern orientation) comprises paths HOT14–HOT27 and HOT27–HOT05 (Fig. 5). The period band 12–100 s was used for the inversion of path HOT14–HOT05. We compare the inversion result of path HOT14–HOT05 with the sum of two narrower frequency band inversions (12–60 s) for paths HOT14–HOT27 and HOT27–HOT05 (Figs 8d, c and b). In a similar way, path HOT15–HOT20 (northerly orientation) is approximately duplicated by the sum of paths HOT15–HOT18 and HOT24–HOT20. Examination of Figs 8(d), (b), (c), 7(c), (d) and (e) shows that the consistency of the results is within ∼1 per cent down to a depth of 150 km.

5 RESULTS

The results are shown in Figs 7 and 8 for the northerly and easterly orientated paths respectively. We use IASP91 as the reference model for the structure between the source and near stations. The panels show percentage differences in V_s relative to the reference model.

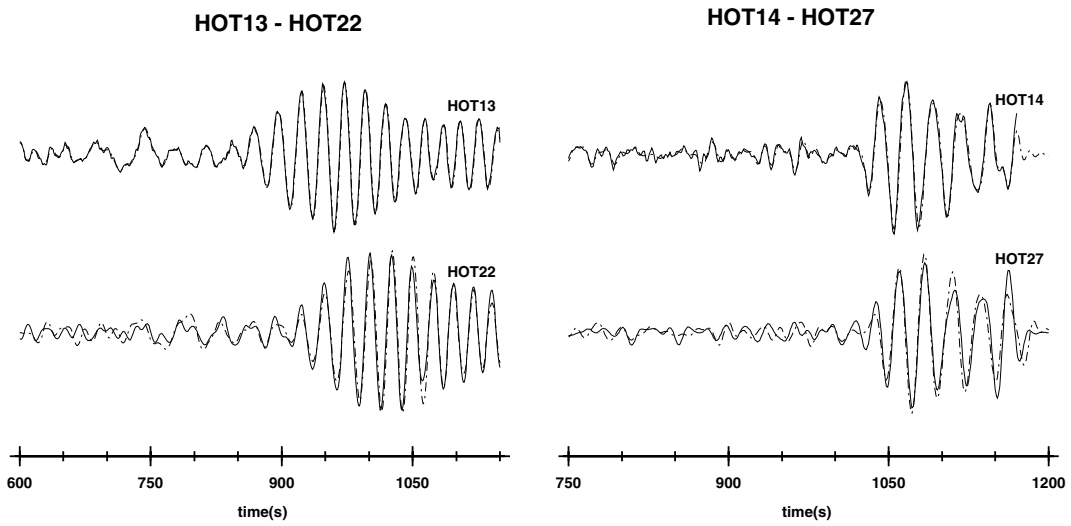

Figure 6. Examples of inversion of real data. Upper panels: fits to the near station waveforms after retrieval of the source term. Lower panels: final fits to the far station waveforms after inversion. Left: path HOT13–HOT22, right: path HOT14–HOT27.

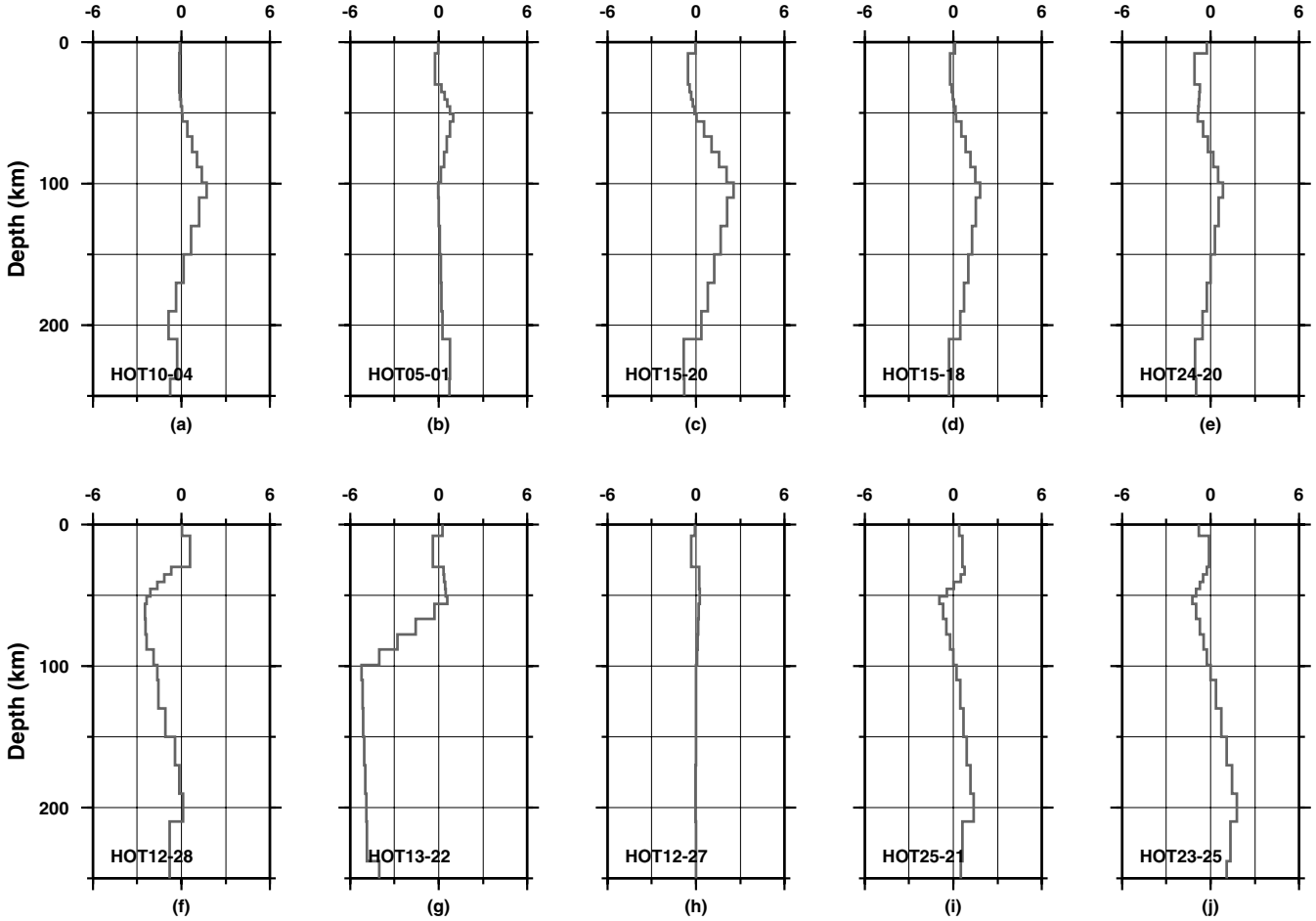

Figure 7. Structures determined from waveform inversion for the northerly orientated paths, shown as percentage differences in V_s relative to the structure beneath the near station. Zero depth refers to the surface.

In order to summarize the results, we divide them on the basis of surface tectonics. Iceland is traversed by a complex neovolcanic zone that forms two branches in south Iceland but only one in north Iceland (Fig. 5). These three northerly orientated branches are connected in central Iceland by a broad east–west trending volcanic zone (the Middle Volcanic Zone), which comprises an array of northerly trending spreading segments. The Northwest Fjords, and western and northern Iceland, comprise intraplate areas and part of the North

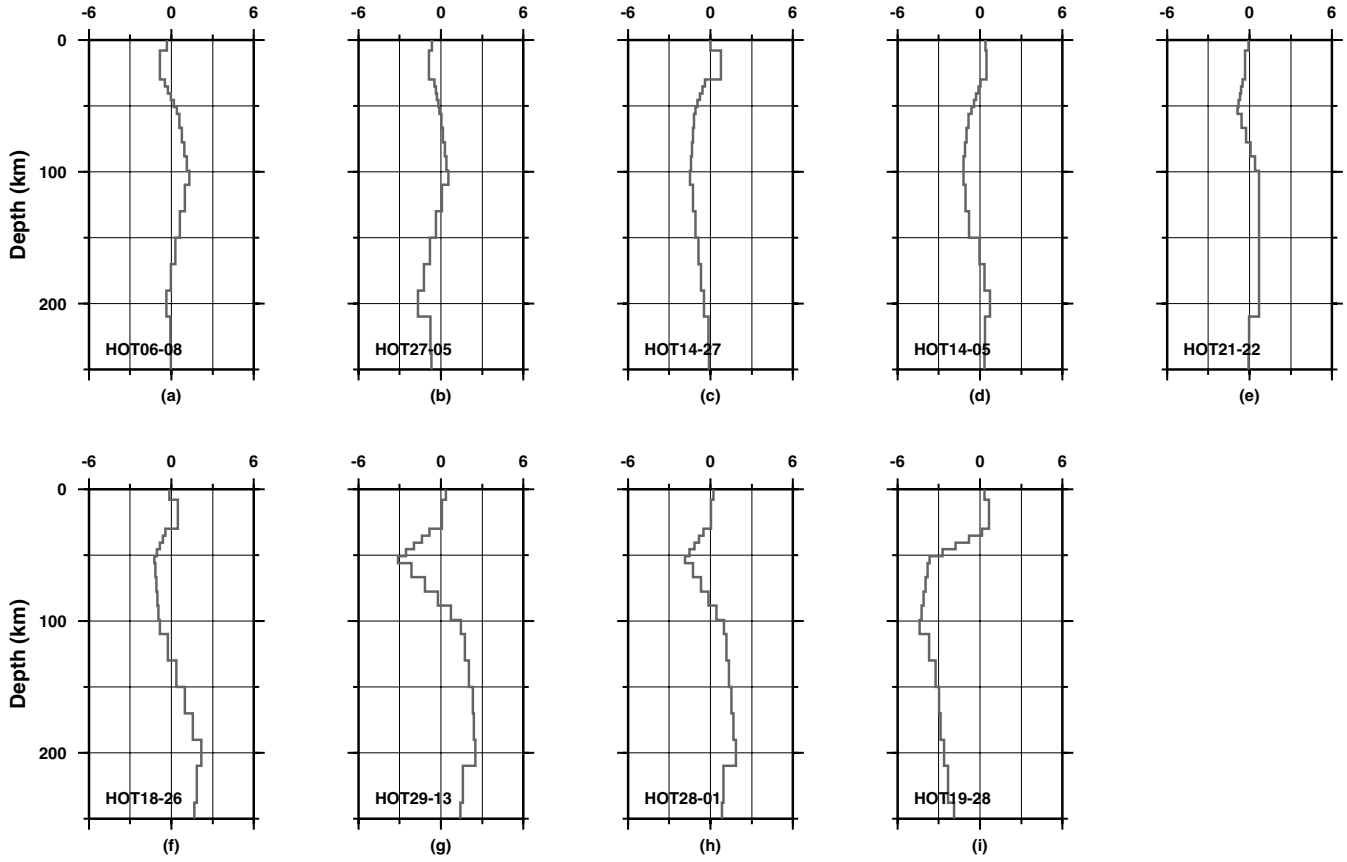

Figure 8. As Fig. 7, but for easterly orientated paths.

American Plate. Eastern Iceland is an intraplate area that is part of the Eurasian Plate. We discuss separately structures beneath the intraplate areas, central Iceland, and the neovolcanic zones away from central Iceland.

The Northwest Fjords area is sampled by paths HOT10–HOT04 (Fig. 7a) and HOT06–HOT08 (Fig. 8a). Both results show relatively high velocities of up to ∼1.5 per cent at depths of ∼100 km. In eastern Iceland, the results of inversions of paths HOT15–HOT20 (Fig. 7c) and HOT15–HOT18 (Fig. 7d) show higher velocities in the depth range ∼50–150 km. The high-velocity anomalies are as large as ∼2.5 per cent in the case of path HOT15–HOT20. We constrain the southern extent of this high-velocity anomaly more tightly with path HOT24–HOT20 (Fig. 7e) which samples the southern part of path HOT15–HOT20. The high velocities are strongest beneath path HOT15–HOT20 and weakest beneath path HOT24–HOT20, suggesting that the structure beneath northeast Iceland is faster than beneath southeast Iceland. Path HOT21–HOT22 (Fig. 8e) samples southeast Iceland, the nature of which is poorly understood as it is covered with Upper Pliocene and younger lavas and sediments. Structure beneath this path shows insignificant variations. In this respect it is most similar to the nearest path in eastern Iceland, HOT24–HOT20 (Fig. 7e).

West and north Iceland are sampled by paths HOT05–HOT01 (Fig. 7b), HOT12–HOT27 (Fig. 7h), HOT27–HOT05 (Fig. 8b), HOT14–HOT27 (Fig. 8c) and HOT14–HOT05 (Fig. 8d). Path HOT14–HOT05 is the longest of these and contains paths HOT14–HOT27 and HOT27–HOT05. We inverted for this path in the period range 12–100 s. Because of the very short station separation distances for other paths, those inversions used data in the period range of 12–60 s only. We detect a minor high-velocity zone beneath path HOT27–HOT05 below ∼50 km, but low velocities beneath HOT14–HOT27 at similar depths, suggesting that the structure beneath station HOT27 may be locally low. On the whole, the lateral variation in structure in this intraplate region is small.

Paths that traverse the neovolcanic zones away from central Iceland include HOT25–HOT21 (Fig. 7i), HOT23–HOT25 (Fig. 7j), HOT18–HOT26 (Fig. 8f), HOT29–HOT13 (Fig. 8g) and HOT28–HOT01 (Fig. 8h). Structures beneath these paths all show shallow low-velocity zones with anomalies as strong as ~ -3 per cent but more typically ~ -2 per cent, in the depth range ∼25–100 km. Beneath this, velocities are consistently higher than beneath the near stations by up to ∼2.5 per cent. Although each structure was independently derived, the results are consistent and different from the structures beneath other Icelandic tectonic regions. Thus, beneath the neovolcanic zones, V_s in the shallow mantle is lower than beneath the surrounding areas, and the reverse is the case deeper than ∼100 km. The most extreme structure is seen beneath path HOT29–HOT13 (Fig. 8g) where the V_s anomaly at ∼50 km depth is as much as ~ -3 per cent. This path crosses the Northern Volcanic Zone beneath the Krafla region.

Central Iceland is sampled by paths HOT12–HOT28 (Fig. 7f), HOT13–HOT22 (Fig. 7g) and HOT19–HOT28 (Fig. 8i). These are the longest paths we studied and the waveform inversion could be conducted for the period range 12–100 s. Only these paths reveal structures with vertically extensive low-velocity zones that extend down to the limit of our resolution at ∼200 km. The top of the low-velocity zone lies at a depth of ∼25–50 km and the anomaly

has a strength of up to ∼ −5 per cent. It is strongest at depths of 50–100 km.

Examination of adjacent paths enables the lateral extent of the low-velocity body beneath central Iceland to be constrained. Its absence beneath both paths HOT14–HOT05 (Fig. 8d) and HOT18–HOT26 (Fig. 8f) shows that it does not extend north of stations HOT27 and HOT14. There is also no sign of it beneath path HOT23–HOT25 (Fig. 7j), which was studied using an event approaching from the south-southwest, path HOT25–HOT21 (Fig. 7i). Both of these paths are underlain by mantle with structure characteristic of that beneath the neovolcanic zones away from central Iceland (Figs 7i, j and Figs 8e, g and h), but have even lower amplitude shallow low-V_s anomalies. This suggests that the deep low-V_s anomaly beneath central Iceland is probably bounded to the north and east by stations HOT27, HOT26, HOT25 and HOT21.

6 COMPARISON WITH TELESEISMIC TOMOGRAPHY

Fig. 9 shows the structure beneath Iceland in the upper 200 km determined using teleseismic traveltime tomography (Foulger *et al.* 2000, 2001). We compare the details with our surface wave waveform inversion results. The surface wave inversions are powerful for targeting specific volumes, but may underestimate the lateral extent of velocity variations where station separations are smaller than the anomalies under investigation. Tomography, on the other hand, is prone to smearing anomalies throughout a larger volume than their true extent.

The agreement between the two sets of results is best beneath central Iceland, where both methods detect low velocities that are continuous throughout the upper ∼200 km. The teleseismic tomography finds that the anomaly amplitude reduces in the depth range ∼100–150 km and strengthens again beneath this. The surface wave waveform inversions do not show such a reduction in the anomaly, however, but show instead that the reduction in anomaly strength below a depth of ∼100 km is gradual. The waning in the strength of the low-velocity anomaly below the upper ∼100–150 km, and subsequent strengthening below this, is nevertheless a feature in many teleseismic tomography inversions performed for both V_p and V_s (e.g. Pritchard 2000). The resolution of the surface wave waveform results is poor at depths >200 km, so comparisons with the results of the teleseismic tomography for such large depths is not meaningful. The surface wave waveform inversions detect maximum velocity contrasts between central Iceland and intraplate areas of up to a total of ∼7 per cent, whereas somewhat smaller maximum anomaly amplitudes of ∼5 per cent were detected by the teleseismic tomography. This lower maximum anomaly amplitude is consistent with the expected distribution of anomalies throughout somewhat larger volumes by teleseismic tomography than surface wave waveform inversions.

The neovolcanic zones away from central Iceland are found by both the teleseismic traveltime tomography and the surface wave waveform inversions to be underlain by low velocities in the upper ∼100 km. The surface wave waveform inversions show that these anomalies do not continue deeper, in contrast to teleseismic tomography, which detects continuation of the low velocities down to ∼150 km beneath the Northern Volcanic Zone. The agreement is best beneath the Western Volcanic Zone (Fig. 5), where both methods find low velocities to be confined to the upper ∼100 km.

Both the surface wave inversions and the tomography agree well beneath eastern Iceland. There, both sets of results show that the area is underlain in general by high velocities which are stronger in the northeast and weaker in the southeast.

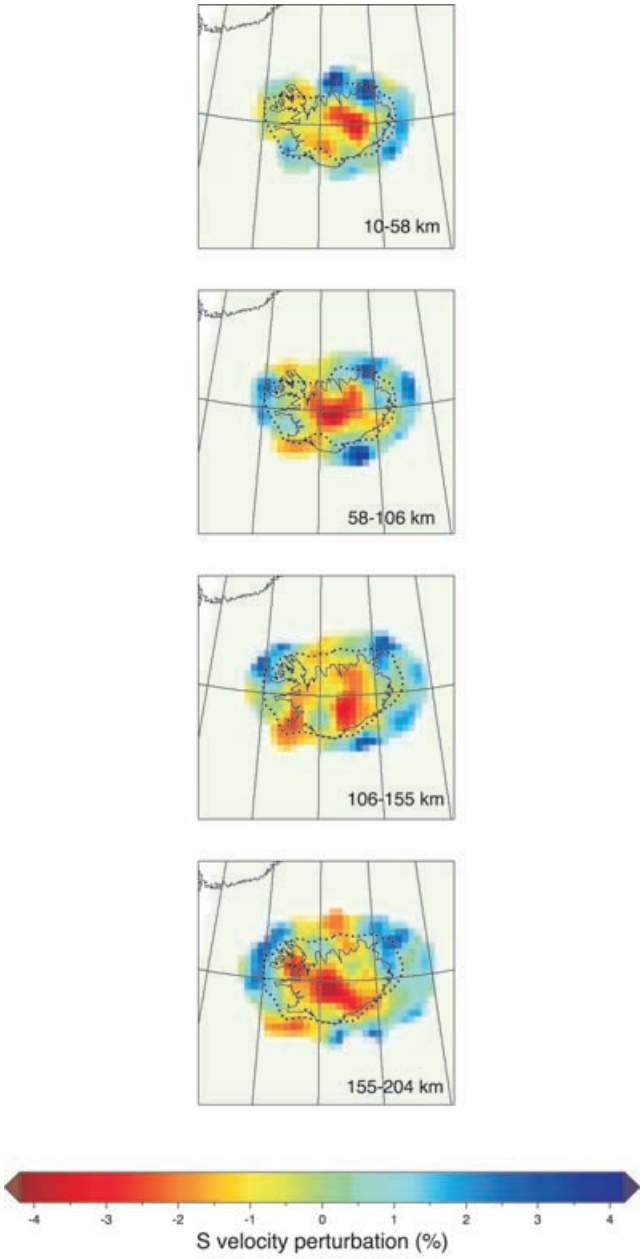

Figure 9. Structure in the upper ∼200 km beneath Iceland determined using teleseismic tomography and the same station network as shown in Fig. 5. Panels show cross-sections through the V_s model at the depth intervals indicted in each panel. From Foulger *et al.* (2001).

This comparison shows that whereas the first-order results of the teleseismic tomography are confirmed, details in the tomography images on the scale of ∼50 km are less reliable. The surface wave waveform results are consistent within a single tectonic province, and provide a conservative indication of the level of detail that is reliable in teleseismic tomography images.

Other teleseismic tomography images of Iceland include those of Tryggvason *et al.* (1983), Wolfe *et al.* (1997) and Allen *et al.* (2002). Fig. 10 shows a comparison of those published V_s images of the shallow upper mantle insofar as is possible given the different depths of published cross-sections and colour scales and reference

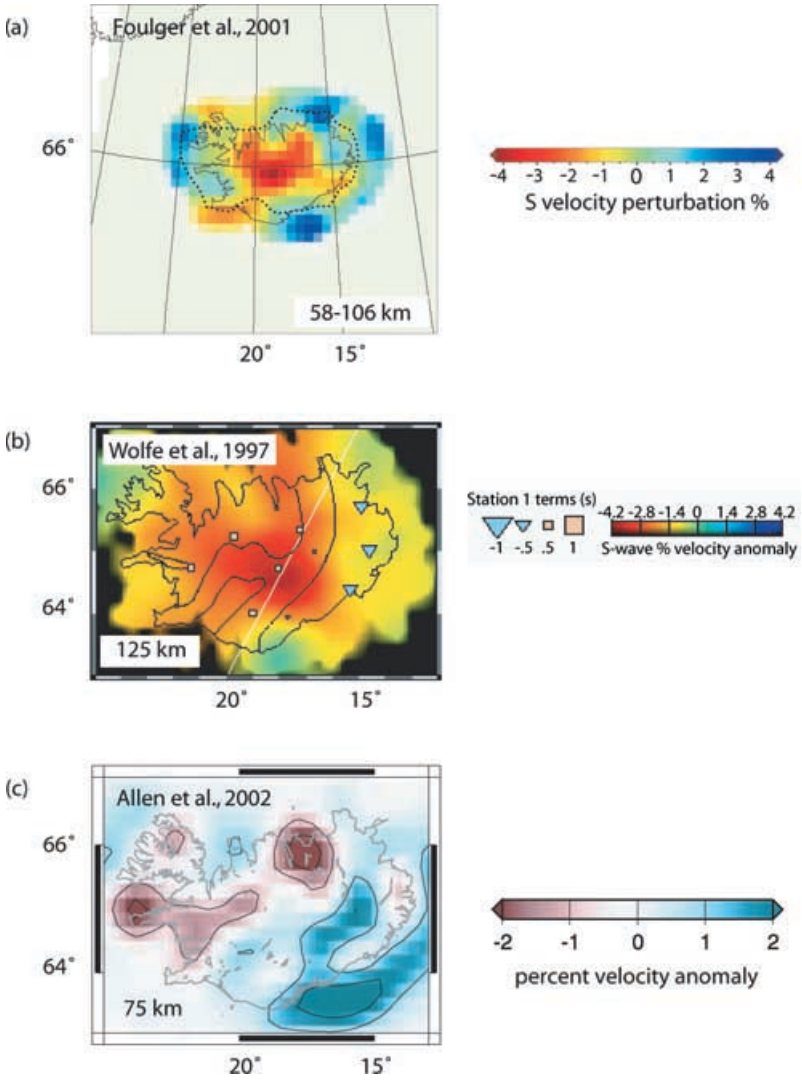

Figure 10. Comparison of horizontal sections through tomographic V_s models of Iceland at similar depths in the shallow mantle. (a) The model of Foulger *et al.* (2001) at 58–106 km depth. (b) The model of Wolfe *et al.* (1997) at 125 km depth. (c) The model of Allen *et al.* (2002) at 75 km depth.

models used. The model of Tryggvason *et al.* (1983) was derived for V_p, and therefore is not suitable for direct comparison with V_s images presented here by others. The V_s image of Allen *et al.* (2002) differs significantly from the other two. Wolfe *et al.* (1997) imaged a strong negative V_s anomaly that extends over a broad, quasi-circular region centred about central Iceland and along the NVZ to the north at ∼125 km. This agrees qualitatively with our surface wave waveform inversion results with the exception that we do not detect the extension of the anomaly along the NVZ at this depth and we find the anomaly beneath central Iceland to be more compact than found by Wolfe *et al.* (1997). This latter discrepancy is to be expected in view of the greater volume averaging inherent in teleseismic tomography.

7 DISCUSSION AND CONCLUSIONS

We present here a new waveform inversion method that involves extending the conventional phase-only two-station waveform inversion method (Kushnir *et al.* 1989). The new method adopts the 'local mode' approximation for surface waves, and can be used for inverting waveforms for structures with not only vertical but also smooth horizontal variations. We apply this new method to obtain upper mantle structure beneath Iceland. Waveforms for a total of 19 station pairs and rays travelling in northerly, easterly and south-southwesterly orientations, sampling all the tectonic areas of Iceland, were used. The use of short ray paths increases the structural resolution achievable but reduces the depth penetration possible. The structural differences between the two stations of each pair correspond directly to the differences between the two waveforms recorded, so this method enables a robust estimate of regional Earth structure to be made.

All inversion methods for retrieving Earth structure from seismograms have advantages and disadvantages. Although we use short paths to overcome the problem of large volume averaging, the relative error for a single path inversion may be large compared with 3D tomographic inversions. In order to overcome this we performed independent inversions using perpendicular ray paths. As is usually the case for tomographic inversions, we neglect the effects of anisotropy and path deviation from the great circle approximation. Because of the non-uniqueness of geophysical inversions, it is important to compare results with those determined using different methods. The

method we present in this paper delivers locally higher resolution than teleseismic tomography since it focuses on specific subsections of the area. It thus provides a useful tool for checking specific details in 3-D tomographic models.

We confirm that a downward-extensive, low-velocity zone occupies at least the upper ∼200 km beneath central Iceland. The depth to the bottom of this zone was not constrained due to the limited penetration depth of the fundamental mode of the surface waves used. This area is the locus of the thickest crust in Iceland, where exceptional values of ∼40 km have been detected (Du & Foulger 2001; Foulger *et al.* 2003). The maximum velocity contrasts in the region we observe are ∼7 per cent at ∼100 km depth. This could be explained by up to ∼1 per cent of partial melt if all the anomaly is interpreted as melt in inclusions with large aspect ratios (Goes *et al.* 2000). An interpretation in terms of temperature would suggest a temperature anomaly of >400 K. This is unlikely because there is no petrological evidence for such a large temperature anomaly. Indeed, the eruptive temperatures estimated for primary melts from central Iceland are only ∼1240 °C (Breddam 2002), which is close to those of similarly magnesian N-MORB (Ford *et al.* 1983). Compositional effects could also be involved, a possibility that is supported by considerable petrological evidence that suggests major heterogeneity in the Icelandic melt source (e.g. Hards *et al.* 1995).

Away from central Iceland, the neovolcanic zones are underlain by low-velocity zones in the upper ∼100 km only, and are thus sourced in the shallow mantle. The neovolcanic zone beneath northwest Vatnajokull, the location traditionally attributed to a mantle plume beneath Iceland, is also found to be underlain by a shallow structure typical of the distal neovolcanic zones. The maximum velocity contrasts with intraplate areas are consistently at ∼50 km depth and may be as strong as ∼5 per cent, corresponding to ∼0.7 per cent partial melt for large-aspect-ratio inclusions (Goes *et al.* 2000). Such structures, and the depth extent of the low-velocity anomalies, are similar to those expected for mid-ocean ridges in general, but confirmation of this must await the acquisition of comparable information about submarine parts of the spreading plate boundary.

ACKNOWLEDGMENTS

This work was supported by Natural Environment Research Council (NERC) grant GR3/10727 and a Sir James Knott Foundation fellowship held by GRF. We thank Jeroen Ritsema and an anonymous referee for their constructive reviews, which led to significant improvements to the manuscript.

REFERENCES

Allen, R.M. *et al.,* 2002. Imaging the mantle beneath Iceland using integrated seismological techniques, *J. geophys. Res.,* **107,** 10.1029/2001JB000595.

Breddam, K., 2002. Kistufell: primitive melt from the Iceland mantle plume, *J. Petrol.,* **43,** 345–373.

Du, Z.J. & Foulger, G.R., 1999. The crustal structure beneath the Northwest Fjords, Iceland, from receiver functions and surface waves, *Geophys. J. Int.,* **139,** 419–432.

Du, Z.J. & Foulger, G.R., 2001. Variation in the crustal structure across central Iceland, *Geophys. J. Int.,* **145,** 246–264.

Du, Z.J. & Panza, G.F., 1999. Amplitude and phase differentiation of synthetic seismograms: a must for waveform inversion at regional scale, *Geophys. J. Int.,* **136,** 83–98.

Du, Z.J. *et al.,* 2002. Crustal structure beneath western and eastern Iceland from surface waves and receiver functions, *Geophys. J. Int.,* **149,** 349–363.

Ford, C.E., Russell, D.G., Craven, J.A. & Fisk, M.R., 1983. Olivine-liquid equilibria: temperature, pressure and composition dependence of the crystal/liquid cation partition coefficients for Mg, Fe^{2+}, Ca, and Mn, *J. Petrol.,* **24,** 256–265.

Foulger, G.R. *et al.,* 2000. The seismic anomaly beneath Iceland extends down to the mantle transition zone and no deeper, *Geophys. J. Int.,* **142,** F1–F5.

Foulger, G.R. *et al.,* 2001. Seismic tomography shows that upwelling beneath Iceland is confined to the upper mantle, *Geophys. J. Int.,* **146,** 504–530.

Foulger, G.R., Du, Z.J. & Julian, B.R., 2003. Icelandic type crust, *Geophys. J. Int.,* **155,** 567–590.

Goes, S., Govers, R. & Vacher, P., 2000. Shallow mantle temperatures under Europe from P and S wave tomography, *J. geophys. Res.,* **105,** 11 153–11 169.

Hards, V.L., Kempton, P.D. & Thompson, R.N., 1995. The heterogeneous Iceland plume—new insights from the alkaline basalts of the Snaefell volcanic Center, *J. Geol. Soc.,* **152,** 1003–1009.

Kennett, B.L.N., 1995. Approximations for surface wave propagation in laterally varying media, *Geophys. J. Int.,* **122,** 470–478.

Kushnir, A.F., Levshin, A.L. & Lokshtanov, D.E., 1989. Determination of a regional velocity structure from surface wave seismograms recorded at a set of stations, in *Proceedings of the Sixth International Mathematical Geophysics Seminar*, Vol. 3, pp. 489–498, Free University, Berlin, Germany.

Levshin, A.L., 1985. Effects of lateral inhomogeneities on surface waves amplitude measurements, *Ann. Geophys. B.,* **3,** 511–518.

Maupin, V. & Kennett, B.L.N., 1987. On the use of truncated modal expansions in laterally varying media, *Geophys. J. Int.,* **91,** 837–851.

Passier, M.L., van der Hilst, R.D. & Snieder, R.K., 1997. Surface wave waveform inversions for local shear-wave velocities under eastern Australia, *Geophys. Res. Lett.,* **24,** 1291–1294.

Pritchard, M.J., 2000. A seismological study of the mantle beneath Iceland, *PhD thesis*, University of Durham, UK.

Ritsema, J., van Heijst, H.J. & Woodhouse, J.H., 1999. Complex shear wave velocity structure imaged beneath Africa and Iceland, *Science,* **286,** 1925–1928.

Tryggvason, K., Husebye, E.S. & Stefansson, R., 1983. Seismic image of the hypothesized Icelandic hot spot, *Tectonophysics,* **100,** 94–118.

Wolfe, C.J., Bjarnason, I.T., VanDear, J.C. & Solomon, S.C., 1997. Seismic structure of the Iceland mantle plume, *Nature,* **385,** 245–247.

Woodhouse, J.H., 1974. Surface waves in a laterally varying layered structure, *Geophys. J. R. astr. Soc.,* **37,** 461–490.